


Assembly and properties of four new metal–organic coordination polymers with flexible bis-pyridyl-bis-amide ligands: effect of aromatic dicarboxylates and central metal ions on the structures

Hongyan Lin, Jian Luan, Xiuli Wang, Guocheng Liu, Aixiang Tian & Juwen Zhang

To cite this article: Hongyan Lin, Jian Luan, Xiuli Wang, Guocheng Liu, Aixiang Tian & Juwen Zhang (2015) Assembly and properties of four new metal–organic coordination polymers with flexible bis-pyridyl-bis-amide ligands: effect of aromatic dicarboxylates and central metal ions on the structures, *Journal of Coordination Chemistry*, 68:1, 71-87, DOI: [10.1080/00958972.2014.983492](https://doi.org/10.1080/00958972.2014.983492)


To link to this article: <http://dx.doi.org/10.1080/00958972.2014.983492>

 View supplementary material 

 Accepted author version posted online: 03 Nov 2014.
Published online: 26 Nov 2014.

 Submit your article to this journal 

 Article views: 69

 View related articles 

 View Crossmark data 

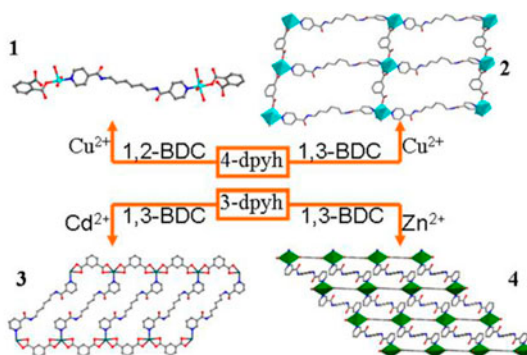
 Citing articles: 5 View citing articles 

Assembly and properties of four new metal–organic coordination polymers with flexible bis-pyridyl-bis-amide ligands: effect of aromatic dicarboxylates and central metal ions on the structures

HONGYAN LIN, JIAN LUAN, XIULI WANG*, GUOCHENG LIU, AIXIANG TIAN and JUWEN ZHANG

Department of Chemistry, Bohai University, Jinzhou, PR China

(Received 4 June 2014; accepted 10 September 2014)



Four new metal–organic coordination polymers have been hydrothermally synthesized by the flexible bis-pyridyl-bis-amide ligands and two different aromatic dicarboxylates. The influences of the different dicarboxylates and central metal ions on the structures of 1–4 have been reported. Moreover, the electrochemical behaviors of 1 and 2, thermal stabilities, and the fluorescent properties of 1–4 have been investigated.

Four coordination polymers, $[\text{Cu}(\text{4-dpyh})_{0.5}(\text{1,2-BDC})(\text{H}_2\text{O})_3] \cdot \text{H}_2\text{O}$ (1), $[\text{Cu}(\text{4-dpyh})(\text{1,3-BDC})(\text{H}_2\text{O})]$ (2), $[\text{Cd}(\text{3-dpyh})_{0.5}(\text{1,3-BDC})(\text{H}_2\text{O})_2] \cdot \text{H}_2\text{O}$ (3), and $[\text{Zn}(\text{3-dpyh})(\text{1,3-BDC})] \cdot 3\text{H}_2\text{O}$ (4) [4-dpyh = *N,N'*-bis(4-pyridinecarboxamide)-1,6-hexane, 3-dpyh = *N,N'*-bis(3-pyridinecarboxamide)-1,6-hexane, 1,2-H₂BDC = 1,2-benzenedicarboxylic acid and 1,3-H₂BDC = 1,3-benzenedicarboxylic acid], have been hydrothermally synthesized. X-ray diffraction analyses reveal that 1 is a discrete $[\text{Cu}_2(\text{4-dpyh})(\text{1,2-BDC})_2]$ dinuclear structure. Compound 2 exhibits a 2-D grid layer constructed from 1-D linear $[\text{Cu}(\text{1,3-BDC})]_n$ chains and $[\text{Cu}(\text{4-dpyh})]_n$ chains. Compound 3 features a 1-D ladder-like chain formed by the 1-D linear $[\text{Cd}(\text{1,3-BDC})]_n$ chains and 3-dpyh bridging ligands. Compound 4 displays a 2-D undulated layer containing meso-helical $[\text{Zn}(\text{3-dpyh})]_n$ chains and linear $[\text{Zn}(\text{1,3-BDC})]_n$ chains. The neighboring dinuclear complexes for 1, adjacent chains for 3, and adjacent layers for 2 and 4 are further linked by hydrogen bonding interactions to form 2-D (for 1) or 3-D supramolecular networks (for 2–4). The influences of the different dicarboxylates and metal on the

*Corresponding author. Email: wangxiuli@bhu.edu.cn

structures of **1–4** have been discussed. The electrochemical behaviors of **1** and **2**, the thermal stabilities and fluorescent properties of **1–4**, and the fluorescent selectivities of **3** and **4** have been investigated.

Keywords: Hydrothermal synthesis; Coordination polymer; Crystal structure; Electrochemical behavior; Fluorescent property

1. Introduction

Metal–organic coordination polymers (MOCPs) are of interest in crystal engineering and materials chemistry, stemming from their intriguing topological frameworks and their potential applications in catalysis, magnetic materials, luminescence, and molecular adsorption [1–4]. A variety of MOCPs with diversified topologies and interesting properties have been obtained by combination of metal ions and organic ligands [5–9]. Mixed-ligand systems based on carboxylates and neutral N-donor ligands have become an effective approach to prepare MOCPs [10–14], allowing modification of architectures and adjusting physical properties of target compounds. For example, Zhang *et al.* reported $[\text{Zn}(\text{L})(\text{bpmp})]_n$ ($\text{H}_2\text{L} = 4,6\text{-dibenzoylisophthalic acid}$; $\text{bpmp} = N,N'\text{-bis}(4\text{-pyridyl-methyl})\text{piperazine}$), which possesses the rare threefold interpenetrating *neb* framework and displays strong luminescence [15]. Up to now, a large number of MOCPs with various structures derived from carboxylates and N-donor ligands have been reported [16–20].

Bis-pyridyl-bis-amide ligands, as N/O-donor ligands, have been utilized to bridge metal ions, leading to new MOCPs with fascinating structures and interesting properties [21–24]. For example, using the semi-rigid bis-pyridyl-bis-amide ligands with benzene-bridging group $[N,N'\text{-bis}(4/3\text{-pyridinecarboxamide})\text{-}1,4\text{-benzene}$ (4/3-bpcb), see scheme S1, see online supplemental material at <http://dx.doi.org/10.1080/00958972.2014.983492> or cyclohexane-bridging group $[N,N'\text{-bis}(3\text{-pyridinecarboxamide})\text{-}1,4\text{-cyclohexane}$ (3-bpcd), see scheme S1) and different aromatic polycarboxylic acids as the mixed-ligands, we have prepared a series of Cu(II)/Co(II) compounds, including 1-D polymeric chain, 2-D layered structures, and 3-D coordination networks [25–27]. By choosing the flexible $N,N'\text{-di}(4\text{-pyridyl})\text{adipoamide}$ ligand (L), Chen's group has obtained two eight- and nine- fold interpenetrating diamondoid networks $\{[\text{Zn}(\text{L})(1,4\text{-BDC})]\cdot\text{H}_2\text{O}\}_n$ and $\{[\text{Cd}(\text{L})(1,4\text{-BDC})]\cdot 2\text{H}_2\text{O}\}_n$ (1,4-H₂BDC = 1,4-benzenedicarboxylic acid) [22]. In our more recent work, we introduced the flexible bis-pyridyl-bis-amide ligand $N,N'\text{-bis}(3\text{pyridinecarboxamide})\text{-}1,6\text{-hexane}$ (3-dpyh) into the metal-BTC ($\text{H}_3\text{BTC} = 1,3,5\text{benzenetricarboxylic acid}$) system and generated a 3-D coordination polymer $[\text{Cu}_4(\text{BTC})_2(3\text{dpyh})(\mu_3\text{-OH})_2(\text{H}_2\text{O})]\cdot 6\text{H}_2\text{O}$ [28]. Compared to the flexible bis-pyridyl-bis-amides with the semi-rigid bis-pyridyl-bis-amides (see scheme S1), the backbones $\text{-(CH}_2\text{)}_6\text{-}$ of $N,N'\text{-bis}(4\text{pyridinecarboxamide})\text{-}1,6\text{-hexane}$ (4-dpyh) or 3-dpyh can bend to larger twist-degree to satisfy the coordination of metal centers, and intriguing structures should be expected.

As an extension of our previous study [25–28], two flexible bis-pyridyl-bis-amide ligands, 4-dpyh and 3-dpyh, are selected as neutral N/O-donors to be introduced into the {metal-dicarboxylate} systems. Four MOCPs, $[\text{Cu}(4\text{-dpyh})_{0.5}(1,2\text{BDC})(\text{H}_2\text{O})_3]\cdot\text{H}_2\text{O}$ (**1**), $[\text{Cu}(4\text{-dpyh})(1,3\text{-BDC})(\text{H}_2\text{O})]$ (**2**), $[\text{Cd}(3\text{-dpyh})_{0.5}(1,3\text{-BDC})(\text{H}_2\text{O})_2]\cdot\text{H}_2\text{O}$ (**3**), and $[\text{Zn}(3\text{-dpyh})(1,3\text{-BDC})]\cdot 3\text{H}_2\text{O}$ (**4**), have been prepared under hydrothermal conditions. The crystal structures of the compounds have been determined and discussed. Thermal properties, electrochemical behaviors, and the fluorescent properties of **1–4** in the solid state have been investigated.

2. Experimental

2.1. Materials and methods

All reagents and solvents for syntheses were purchased from commercial sources and used without purification. The 4-dpyh and 3-dpyh were prepared according to reported procedures [29]. FT-IR spectra (KBr pellets) were taken on a Varian FT-IR 640 spectrometer by KBr pellets from 4000 to 500 cm^{-1} . Thermogravimetric analyses (TGA) were performed on a SDT 2960 simultaneous DSC-TGA instrument under flowing N_2 with a heating rate of 10 $^\circ\text{C min}^{-1}$. Powder X-ray diffraction (PXRD) investigations were carried out with an Ultima IV with D/teX Ultra diffractometer at 40 kV, 40 mA with Cu $\text{K}\alpha$ ($\lambda = 1.5406 \text{ \AA}$) radiation. The electrochemical experiments were carried out with a CHI 440 Electrochemical Quartz Crystal Microbalance. A conventional three-electrode cell was used at room temperature. Compounds **1** and **2** bulkmodified carbon paste electrodes (**1**-CPE and **2**-CPE), were used as working electrodes. An SCE and a platinum wire were used as reference and auxiliary electrodes, respectively. The bulk-modified CPEs were fabricated with methods from the literature [25]. Fluorescence spectra were recorded in solid state at room temperature on a Hitachi F-4500 fluorescence/phosphorescence spectrophotometer.

2.2. Preparation of 1–4

2.2.1. Synthesis of $[\text{Cu}(4\text{-dpyh})_{0.5}(\text{1,2-BDC})(\text{H}_2\text{O})_3]\cdot\text{H}_2\text{O}$ (1**).** A mixture of $\text{CuCl}_2\cdot 2\text{H}_2\text{O}$ (0.034 g, 0.2 mM), 4-dpyh (0.033 g, 0.1 mM), 1,2- H_2BDC (0.025 g, 0.15 mM), H_2O (12 mL), and NaOH (0.015 g, 0.38 mM) was stirred for 30 min, at room temperature. The suspension was transferred to a Teflon-lined autoclave (25 mL) and kept at 120 $^\circ\text{C}$ for 4 days. After slow cooling to room temperature, blue block crystals of **1** were obtained, filtered, and the blue precipitate washed off with ethanol. Yield 37% based on Cu. Anal. Calcd for $\text{C}_{17}\text{H}_{23}\text{CuN}_2\text{O}_9$: C, 44.07; H, 4.97; N, 6.05. Found: C, 44.09; H, 4.99; N, 6.01%. IR (KBr pellet, cm^{-1}): 3357 (s), 2939 (m), 1649 (s), 1606 (s), 1546 (s), 1500 (m), 1477 (m), 1429 (m), 1361 (s), 1307 (m), 1228 (w), 1070 (w), 864 (w), 742 (m), 696 (m), 617 (m), 582 (w), 532 (w).

2.2.2. Synthesis of $[\text{Cu}(4\text{-dpyh})(\text{1,3-BDC})(\text{H}_2\text{O})]\text{ (2)}$. Complex **2** was prepared in the same way as **1** except that 1,3- H_2BDC (0.025 g, 0.15 mM) was used instead of 1,2- H_2BDC and a different amount of NaOH (0.016 g, 0.40 mM) was added to adjust the pH of the reaction mixture. Blue block crystals of **2** were obtained, filtered, and the blue precipitate washed off with ethanol. Yield: 32% based on Cu. Anal. Calcd for $\text{C}_{26}\text{H}_{28}\text{CuN}_4\text{O}_7$: C, 54.54; H, 4.89; N, 9.79. Found: C, 54.47; H, 4.92; N, 9.71%. IR (KBr pellet, cm^{-1}): 3368 (m), 2341 (m), 1651 (s), 1635 (m), 1616 (m), 1558 (s), 1541 (s), 1521 (m), 1506 (m), 1475 (m), 1458 (w), 1419 (w), 1361 (m), 1303 (w), 1226 (w), 1070 (m), 862 (w), 744 (w), 671 (m), 515 (w).

2.2.3. Synthesis of $[\text{Cd}(3\text{-dpyh})_{0.5}(\text{1,3-BDC})(\text{H}_2\text{O})_2]\cdot\text{H}_2\text{O}$ (3**).** A mixture of $\text{CdCl}_2\cdot 2.5\text{H}_2\text{O}$ (0.046 g, 0.2 mM), 3-dpyh (0.033 g, 0.1 mM), 1,3- H_2BDC (0.025 g, 0.15 mM), H_2O (12 mL), and NaOH (0.016 g, 0.40 mM) was stirred for 30 min, at room temperature. The suspension was transferred to a Teflon-lined autoclave (25 mL) and kept

at 120 °C for 4 days. Colorless block crystals of **3** were obtained, filtered, and the white precipitate washed off with ethanol. Yield: 32% based on Cd. Anal. Calcd for $C_{17}H_{21}CdN_2O_8$: C, 41.32; H, 4.25; N, 5.67. Found: C, 41.38; H, 4.14; N, 5.58%. IR (KBr pellet, cm^{-1}): 3332 (s), 2935 (m), 2313 (w), 1659 (s), 1604 (s), 1547 (s), 1478 (m), 1444 (m), 1390 (s), 1323 (m), 1227(w), 1167 (m), 1116 (m), 1064 (w), 943 (w), 845 (w), 823 (w), 730 (m), 545 (w).

2.2.4. Synthesis of [Zn(3-dpyh)(1,3-BDC)]·3H₂O (4). The synthesis method of **4** is similar to that of **3** except for $Zn(NO_3)_2 \cdot 6H_2O$ as the substitute of $CdCl_2 \cdot 2.5H_2O$. Colorless block crystals of **4** were obtained, filtered, and washed off the white precipitate with ethanol. Yield: 34% based on Zn. Anal. Calcd for $C_{26}H_{32}ZnN_4O_9$: C, 51.15; H, 5.25; N, 9.18. Found: C, 51.16; H, 5.34; N, 9.09%. IR (KBr pellet, cm^{-1}): 3264 (s), 2935 (m), 2361 (w), 1652 (s), 1615 (s), 1586 (m), 1559 (s), 1479 (m), 1427 (m), 1380 (s), 1364 (s), 1320 (s), 1276 (w), 1224 (w), 1167 (m), 1067 (w), 961 (w), 836 (m), 730 (m), 618 (w), 564 (w).

2.3. X-ray crystallographic studies

Crystallographic data for **1–4** were collected on a Bruker SMART APEX II with Mo K α radiation ($\lambda = 0.71073 \text{ \AA}$) by ω and θ scan mode, at 296 K. The structures were solved by direct methods and refined on F^2 by full-matrix least-squares using the SHELXL package [30]. In **2**, the 4-dpyh and the 1,3-BDC ligands are disordered and the C12, C13, C21, C22, C23, N4, and O6 positions were refined with half occupancy. For **1–4**, a summary of crystal data and structure refinements is provided in table 1. Selected bond distances and angles are listed in table S1. Hydrogen bonding geometries of **1–4** are summarized in table S2.

Table 1. The crystal data and structure refinement for **1–4**.

Complex	1	2	3	4
Empirical formula	$C_{17}H_{23}CuN_2O_9$	$C_{26}H_{28}CuN_4O_7$	$C_{17}H_{21}CdN_2O_8$	$C_{26}H_{32}ZnN_4O_9$
Formula weight	462.91	572.06	493.76	609.93
Crystal system	Triclinic	Triclinic	Triclinic	Monoclinic
Space group	<i>P</i> -1	<i>P</i> -1	<i>P</i> -1	<i>P</i> 2/ <i>c</i>
<i>a</i> (Å)	7.4273(7)	10.28(3)	10.2582(9)	10.1435(8)
<i>b</i> (Å)	8.2425(8)	10.77(3)	10.3766(10)	9.7661(8)
<i>c</i> (Å)	16.4803(16)	13.37(4)	10.9877(9)	14.8772(12)
α (°)	85.231(2)	101.10(5)	85.791(2)	90
β (°)	81.759(2)	101.85(5)	75.5200(10)	108.2170(10)
γ (°)	80.405(2)	98.51(5)	61.4290(10)	90
<i>V</i> (Å ³)	982.71(16)	1395(7)	993.07(15)	1399.9(2)
<i>Z</i>	2	2	2	2
<i>D</i> _{calcd} (g cm ⁻³)	1.564	1.362	1.651	1.447
μ (mm ⁻¹)	1.164	0.832	1.145	0.936
<i>F</i> (0 0 0)	480	594	498	636
Reflections collected	5931	6805	5114	6917
Unique reflections	4039	4718	3497	2463
Parameters	262	369	253	183
<i>R</i> _{int}	0.0172	0.0336	0.0155	0.0188
GOF	1.111	1.015	1.064	1.092
<i>R</i> ₁ ^a [<i>I</i> > 2 σ (<i>I</i>)]	0.0401	0.0817	0.0264	0.0299
<i>wR</i> ₂ ^b (all data)	0.1219	0.2477	0.0613	0.0823

^a $R_1 = \sum ||F_o| - |F_c|| / \sum |F_o|$.

^b $wR_2 = \sum [w(F_o^2 - F_c^2)^2] / \sum [w(F_o^2)^2]^{1/2}$.

3. Results and discussion

3.1. Design and syntheses

Many factors can influence the crystallization and structural formation of MOCPs under hydrothermal conditions such as initial reactants, reactant ratio, temperature, pH value, etc. By utilizing the flexible bis-pyridyl-bis-amide 3-dpyh and aromatic polycarboxylates, we obtained a 3-D compound $[\text{Cu}_4(\text{BTC})_2(3\text{-dpyh})(\mu_3\text{-OH})_2(\text{H}_2\text{O})]\cdot 6\text{H}_2\text{O}$ based on two kinds of tetranuclear copper clusters [28], two 2-D networks $[\text{Cu}(3\text{-dpyh})_{0.5}(1,2\text{-BDC})]\cdot \text{H}_2\text{O}$, and $[\text{Cu}(3\text{-dpyh})_{0.5}(5\text{-AIP})(\text{H}_2\text{O})]$ [31]. In order to further investigate the effect of different factors on the assembly of MOCPs, we attempted to synthesize the complexes by choosing different bis-pyridyl-bis-amide 4-dpyh, polycarboxylates, metal ions, and adjusting the pH of reaction system. By using 4-dpyh in place of 3-dpyh, we expected to construct a new compound in similar conditions to that reported [20]. However, in the reaction system containing 4-dpyh and 1,3,5-BTC, by adjusting the reactant ratio and pH, no crystalline product could be isolated, which may be ascribed to the different ligands. So we introduced 1,2-H₂BDC (or 1,3-H₂BDC) into the Cu-4-dpyh system. Only when the reactant ratio (Cu : 1,2-H₂BDC(or 1,3-H₂BDC):4-dpyh) was changed to 2 : 1.5 : 1.0 (same as that in reference [31], the ratio of Cu : dicarboxylate : 3-dpyh is 2 : 1.5 : 1.0), a discrete dinuclear structure $[\text{Cu}(4\text{-dpyh})_{0.5}(1,2\text{-BDC})(\text{H}_2\text{O})_3]\cdot \text{H}_2\text{O}$ (**1**) and a 2-D grid layer $[\text{Cu}(4\text{-dpyh})(1,3\text{-BDC})(\text{H}_2\text{O})]$ (**2**) could be prepared, which are different from that of $[\text{Cu}(3\text{-dpyh})_{0.5}(1,2\text{-BDC})]\cdot \text{H}_2\text{O}$ [31]. For **1** and **2**, the amounts of NaOH (0.38 mM for **1**, 0.40 mM for **2**) are optimal because the slightly changed amount of NaOH can effectively adjust the system pH, which may result in changes of crystal yields for **1** and **2**. In fact, parallel experiments show that our experimental procedures have good repeatability.

To further investigate the effect of metal ions on the structures, we extended our studies from Cu(II) to Cd(II) and Zn(II). However, in the system of 4-dpyh and 1,2-H₂BDC/1,3-H₂BDC, by adjusting the reactant ratio and pH, we cannot obtain any crystalline compound. For the system of 3-dpyh and 1,3-H₂BDC, by adjusting the reactant ratio and pH, two new Cd(II) and Zn(II) compounds are obtained: a 1-D ladder-like chain $[\text{Cd}(3\text{-dpyh})_{0.5}(1,3\text{-BDC})(\text{H}_2\text{O})_2]\cdot \text{H}_2\text{O}$ (**3**) and a 2-D undulated layer $[\text{Zn}(3\text{-dpyh})(1,3\text{-BDC})]\cdot 3\text{H}_2\text{O}$ (**4**). In this article, four new compounds with different structures are generated using different ligands, various metal ions, and adjusting pH, which implies that the crystallization conditions are important, because the syntheses of the compounds are affected not only by the stoichiometries of the reactants but also by the types of co-ligands and the pH of the reaction media [32].

3.2. Descriptions of crystal structures for 1–4

3.2.1. $[\text{Cu}(4\text{-dpyh})_{0.5}(1,2\text{-BDC})(\text{H}_2\text{O})_3]\cdot \text{H}_2\text{O}$ (1**).** Single-crystal X-ray diffraction analysis reveals that the fundamental structure unit in **1** consists of one Cu(II), half of 4-dpyh, one 1,2-BDC anion, three coordinated waters, and one lattice water. As shown in figure 1(a), the crystallographically independent Cu1 is five-coordinate by one pyridyl from a 4-dpyh, one carboxylic oxygen of a 1,2-BDC, and three coordinated waters, completing a $[\text{CuO}_4\text{N}]$ distorted tetragonal pyramidal geometry. The bond lengths of Cu1–N1, Cu1–O2, Cu1–O1 W, Cu1–O2 W, and Cu1–O3 W are 2.014(3), 1.981(2), 1.972(2), 2.292(2), and 1.955(2) Å, respectively. In **1**, 1,2-BDC displays one monodentate coordination mode [see chart

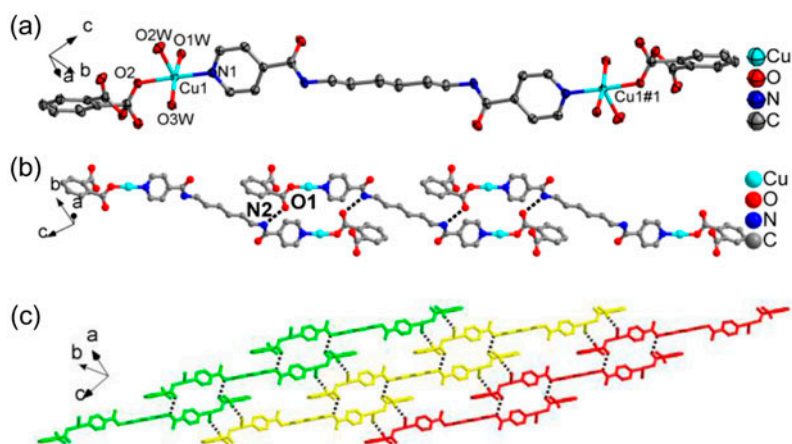


Figure 1. (a) ORTEP drawing of **1** with thermal ellipsoids at 50% probability. The lattice water molecules and hydrogens have been omitted for clarity; (b) the 1-D supramolecular chain in **1**; and (c) view of the 2-D supramolecular layer of **1**.

1(a)] with only one carboxyl group coordinated with Cu1. The 4-dpyh is bidentate, bridging two Cu(II) ions to form a discrete $[\text{Cu}_2(4\text{-dpyh})(1,2\text{-BDC})_2]$ dinuclear structure with the $\text{Cu}\cdots\text{Cu}$ distance of 21.98 Å, in which the corresponding dihedral angle between the pyridyl rings is 0° [see chart 1(b)]. Adjacent dinuclear Cu(II) units are connected through hydrogen bonding interactions between the amide of 4-dpyh ligands and carboxylic oxygen ($\text{N}2\cdots\text{O}1 = 3.082$ Å) to generate a 1-D supramolecular chain as shown in figure 1(b). These 1-D chains are further extended into a 2-D supramolecular layer through $\text{O}1\text{ W}\cdots\text{O}4$ hydrogen bonding interaction between the coordinated water molecules and carboxylic oxygen ($\text{O}1\text{ W}\cdots\text{O}4 = 2.636$ Å) [figure 1(c)].

3.2.2. [Cu(4-dpyh)(1,3-BDC)(H₂O)] (2). When 1,2-H₂BDC ligand was replaced by 1,3-H₂BDC, **2** with a complicated 2-D network was obtained. As shown in figure 2(a), Cu1 is five-coordinate $[\text{CuO}_3\text{N}_2]$ and ligated by two nitrogens from two different 4-dpyh ligands ($\text{Cu}1\text{-N}1 = 2.053(7)$ and $\text{Cu}1\text{-N}2\#2 = 2.054(7)$ Å) and three oxygens from two 1,3-BDC anions and one coordinated water ($\text{Cu}1\text{-O}1 = 2.016(6)$, $\text{Cu}1\text{-O}4\#1 = 2.011(6)$, and $\text{Cu}1\text{-O}1\text{ W} = 2.457(7)$ Å). The 4-dpyh, as a bidentate ligand [see chart 1(d)], links Cu(II) ions to generate a 1-D $[\text{Cu}(4\text{-dpyh})]_n$ linear chain [figure S1(a)], in which the non-bonding distance of $\text{Cu}\cdots\text{Cu}$ is 22.71 Å. The dihedral angle between two pyridyl rings is 73.12° . The 1,3-BDC anion adopts a bis(monodentate) coordination [see chart 1(c)], bridging adjacent Cu(II) ions to form a 1-D linear $[\text{Cu}(1,3\text{-BDC})]_n$ chain with $\text{Cu}\cdots\text{Cu}$ non-bonding distance of 10.28 Å [figure S1(b)]. In this manner, the $[\text{Cu}(4\text{-dpyh})]_n$ chains and $[\text{Cu}(1,3\text{-BDC})]_n$ chains are joined by the Cu(II) ions to yield a 2-D polymeric framework [figure 2(b)]. $\text{O-H}\cdots\text{O}$ and $\text{N-H}\cdots\text{O}$ hydrogen bonding interactions can be observed among neighboring layers, resulting in formation of a 3-D supramolecular network of **2**. The $\text{O-H}\cdots\text{O}$ hydrogen bonding interaction is between coordinated water ($\text{O}1\text{ W}$) and amide oxygen ($\text{O}5$) [$\text{O}(1\text{ W})\cdots\text{O}(5)$, 2.995 Å]. The $\text{N-H}\cdots\text{O}$ hydrogen bonding interaction is between amide nitrogen of 4-bpyh and carboxyl oxygen with $\text{N}(3)\cdots\text{O}(2)$ distance of 3.052 Å [figure 2(c)].

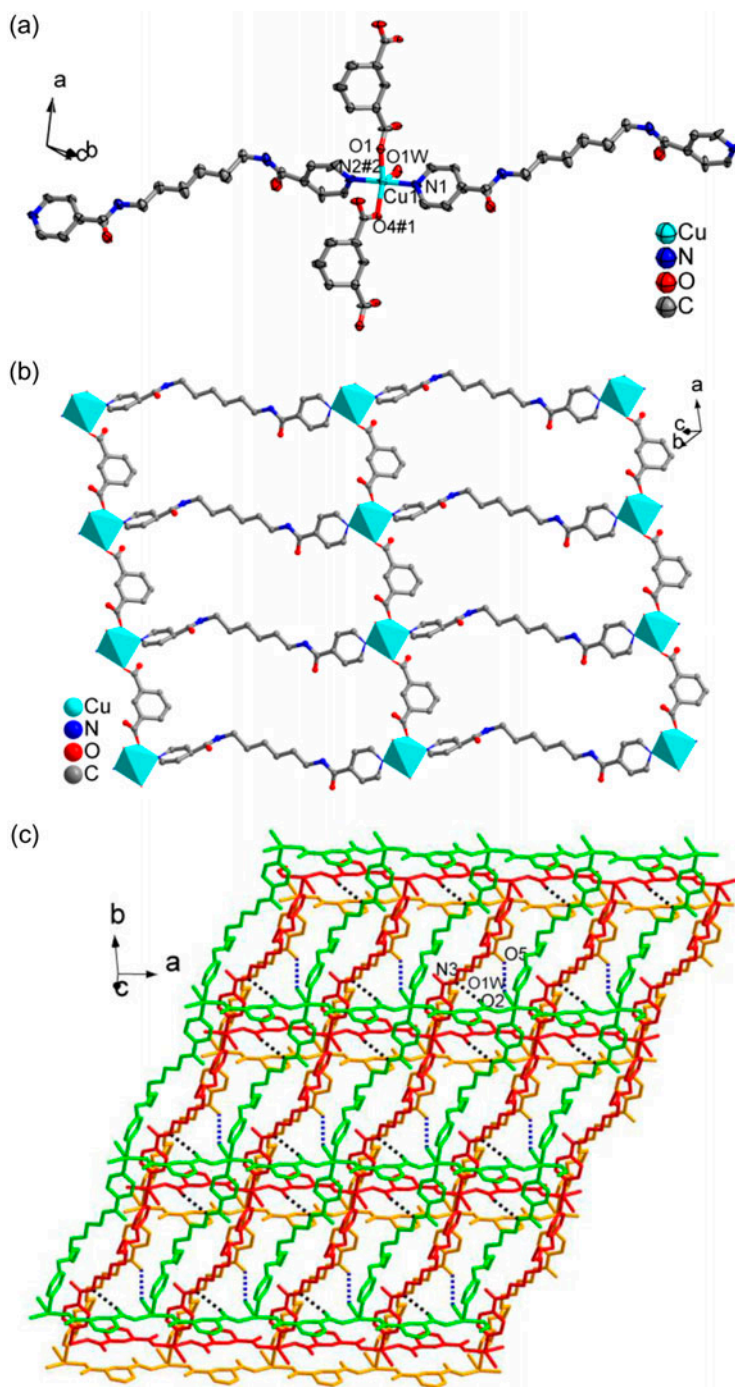


Figure 2. (a) ORTEP drawing of **2** with thermal ellipsoids at 50% probability. The lattice water molecules and hydrogens have been omitted for clarity; (b) the 2-D polymeric layer of **2**; and (c) the 3-D supramolecular framework in **2**.

3.2.3. [Cd(3-dpyh)_{0.5}(1,3-BDC)(H₂O)₂·H₂O (3). The fundamental building block of **3** consists of one Cd(II), half of one 3-dpyh, one 1,3-BDC, two coordinated waters, and one lattice water. The crystallographically independent Cd(1) is seven-coordinate by four carboxyl oxygens from two 1,3-BDC anions (Cd1–O1 = 2.319(2) Å, Cd1–O2 = 2.620(2) Å, Cd1–O3 = 2.5807(19) Å, and Cd1–O4 = 2.3105(19) Å), two oxygens from two coordinated waters (Cd1–O1 W = 2.3176(19) Å and Cd1–O2 W = 2.3070(19) Å), and one nitrogen from one 3-dpyh ligand (Cd1–N1 = 2.319(2) Å) [figure 3(a)]. Neighboring Cd(II) ions are bridged by 1,3-BDC anions to generate a [Cd(1,3-BDC)]_n chain as illustrated in figure 3(b), in which both carboxyl groups of the 1,3-BDC anion chelate [see chart 1(e)]. Then, such 1-D chains are further extended into a 1-D ladder-like chain structure through the bidentate 3-dpyh ligands [chart 1(f)] with Cd···Cd distance of 20.24 Å. Two pyridyl rings of each 3-dpyh ligand are parallel. The intermolecular hydrogen bonding interactions between the carboxyl group and coordinated water can be observed (O1···O1 W = 2.749 Å), which extends the 1-D ladder-like chains into a 2-D supramolecular structure [figure 3(c)]. Furthermore, adjacent 2-D supramolecular layers are connected by hydrogen bonding interactions between the amide nitrogens of 3-dpyh and coordinated waters (N2···O2 W = 2.980 Å) to build a 3-D supramolecular framework, as shown in figure 3(d).

3.2.4. [Zn(3-dpyh)(1,3-BDC)]·3H₂O (4). As CdCl₂·2.5H₂O was replaced by the Zn(NO₃)₂·6H₂O, **4** was obtained. X-ray diffraction analysis reveals that **4** is a 2-D undulated layer. As shown in figure 4(a), each Zn(II) is four-coordinate in a distorted tetrahedral coordination geometry, completed by two nitrogens from two distinct 3-dpyh ligands (Zn1–N1 and Zn1–N1#1, 2.0516(17) Å) and two oxygens from two different 1,3-BDC anions (Zn1–O1 and Zn1–O1#1, 1.9755(14) Å). O2 and O2#1 from bridging 1,3-BDC did not coordinate to Zn1, but presents weak interaction [Zn1···O2 and Zn1···O2#1, 2.6868(17) Å]. Considering the above weak interaction, Zn1 displays a six-coordinate distorted octahedral arrangement in **4**.

Similar to **3**, two carboxyl groups of 1,3-BDC anion adopt chelate [see chart 1(g)], linking the adjacent Zn(II) ions to give a 1-D [Zn(1,3-BDC)]_n linear chain [figure S2(a)]. Each 3-dpyh as a bidentate ligand [chart 1(h)] bridges the Zn(II) ions to build a 1-D [Zn(3-dpyh)]_n meso-helical chain [figure S2(b)]. The combination of [Zn(3-dpyh)] chains and [Zn(1,3-BDC)]_n chains leads to a 2-D undulated layer [figure 4(b)]. Additionally, these adjacent 2-D layers also pack to construct a 3-D supramolecular network with N–H···O hydrogen bonding interactions (N2–H2B···O1 W, 2.820 Å) and O–H···O hydrogen bonding interactions (O2–H1 WA···O1W, 2.774 Å) [figure 4(c)].

Comparing **3** and **4** with the 1-D chain coordination polymers {[Zn(1,3BDC)(bmt)H₂O]·0.5H₂O}_n and {[Cd(1,3-BDC)(bmt)(H₂O)₂]·2H₂O}_n (bmt = 1-((benzotriazol-1yl)methyl)-1-H-1,2,4-triazole) [33], although they are prepared in the same systems of metal ions (Zn(II) and Cd(II)) and dicarboxylate 1,3-BDC, their final framework structures are different. In **3** and **4**, 3-dpyh is bidentate bridging adjacent metal ions. In reference [33], bmt is unidentate and hangs at two sides or one side of the metal-1,3-BDC main chains. The structural diversities of these compounds may be attributed to the differences of N-donor ligands.

3.3. Discussion

We prepared four Cu(II), Cd(II), and Zn(II) compounds based on isomeric bis-pyridyl-bis-amide ligands 4-dpyh/3-dpyh and dicarboxylic acids (1,2-H₂BDC or 1,3-H₂BDC). Our

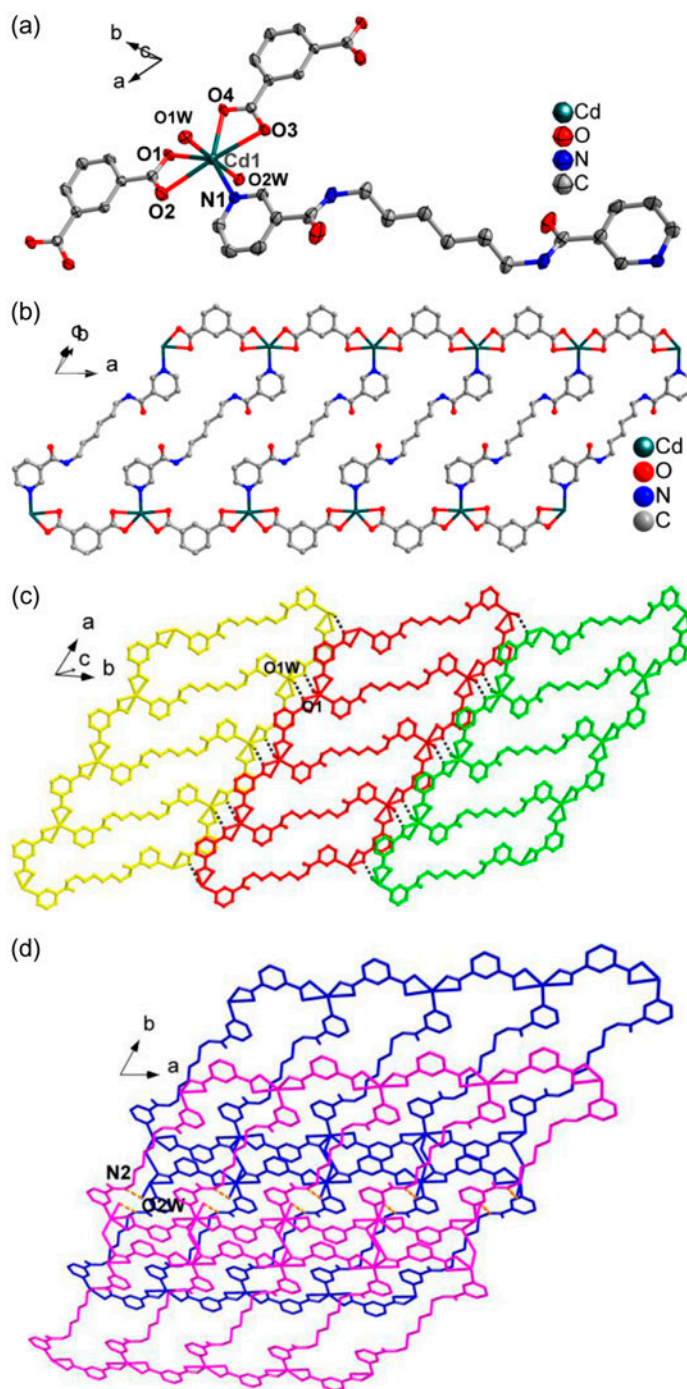


Figure 3. (a) ORTEP drawing of **3** with thermal ellipsoids at 50% probability. The lattice water molecules and hydrogens have been omitted for clarity; (b) view of the 1-D ribbon in **3**; (c) the 2-D supramolecular layer of **3**; and (d) the 3-D supramolecular framework in **3**.

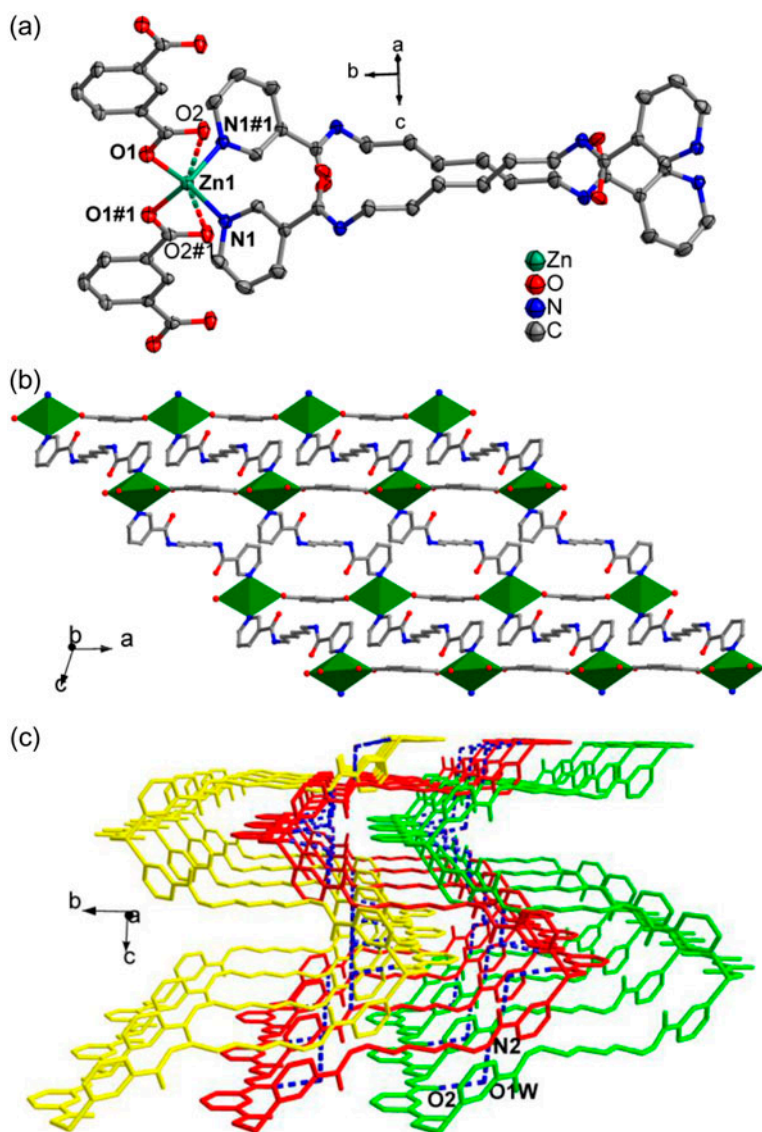


Figure 4. (a) ORTEP drawing of **4** with thermal ellipsoids at 50% probability. The lattice waters and hydrogens have been omitted for clarity; (b) view of the 2-D layer of **4**; and (c) the 3-D supramolecular network in **4**.

results indicate that both different coordination modes of the aromatic dicarboxylates (1,2-H₂BDC or 1,3-H₂BDC) and the central metal ions show obvious effect on the final structures of **1–4**.

3.3.1. Effect of the dicarboxylates on structures 1–4. For **1** and **2** based on Cu(II) and 4-dpyh, different aromatic dicarboxylates show obvious influence on their final structures. In **1** and **2**, 4-dpyh adopts the same bidentate coordination mode linking Cu(II) ions to form

a dinuclear $[\text{Cu}_2(4\text{-dpyh})]$ subunit (for **1**) or a 1-D $[\text{Cu}(4\text{-dpyh})]_n$ linear chain (for **2**). In **1**, 1,2-BDC is monodentate and does not bridge, thus resulting in the final discrete dinuclear structure $[\text{Cu}_2(4\text{-dpyh})(1,2\text{-BDC})_2]$. While in **2**, 1,3-BDC exhibits a bis(monodentate) coordination mode, bridging the Cu(II) ions of adjacent $[\text{Cu}(4\text{-dpyh})]_n$ chains to build a 2-D layer.

3.3.2. Effect of the central metal ions on the structures of 1–4. When 3-dpyh and 1,3-BDC were chosen in **3** and **4**, Cd(II) and Zn(II) complexes with different structures were obtained. For **3** and **4**, the 3-dpyh ligands show the same bidentate bridging mode, and the 1,3-BDC ligands display the same bis(chelate) bridging coordination. In **3**, Cd(II) is seven-coordinate, connected by 1,3-BDC and 4-dpyh ligands to build a ladder-like chain. While in **4**, the Zn(II) is six-coordinate distorted octahedral arrangement (containing two weak $\text{Zn1}\cdots\text{O2}$ and $\text{Zn1}\cdots\text{O2\#1}$ interactions, 2.6868(17) Å) and is linked by 1,3-BDC and 4-dpyh ligands to give 2-D layers. The results indicate the Cd(II) and Zn(II) affect the final structures.

3.4. IR spectra of 1–4

The IR spectra of **1–4** are determined from 500 to 4000 cm^{-1} (figure S3). Strong peaks at 1606 and 1228 cm^{-1} for **1**, 1616 and 1226 cm^{-1} for **2**, 1604 and 1227 cm^{-1} for **3**, and 1615 and 1224 cm^{-1} for **4** may be attributed to asymmetric and symmetric vibrations of carboxyl groups. The bands around 1649 cm^{-1} for **1**, 1651 cm^{-1} for **2**, 1659 cm^{-1} for **3**, and 1652 cm^{-1} for **4** are characteristic of the carbonyl groups. The presence of bands at 1546, 1477, 1429, and 1361 cm^{-1} for **1**, 1558, 1475, 1458, and 1361 cm^{-1} for **2**, 1547, 1478, 1444, and 1390 cm^{-1} for **3**, and 1559, 1479, 1427, and 1380 cm^{-1} for **4** suggest the $\nu_{\text{C-N}}$ stretching vibrations of the pyridyl ring of the 4-dpyh or 3-dpyh ligands. For **1–4**, the strong absorptions at 3357, 3368, 3332, and 3264 cm^{-1} indicate the presence of –OH groups of water.

3.5. Powder X-ray diffraction

The crystal phase purities of **1–4** were evidenced by the similarity of the simulated and experimental PXRD patterns, as shown in figure S4. The as-synthesized crystal patterns are in agreement with the corresponding simulated ones, indicating the phase purities of the as-synthesized crystalline samples.

3.6. Thermal analyses

The coordination frameworks for **1–4** are air-stable, and their thermal stabilities are studied under nitrogen by TGA with a heating rate of 10 $^{\circ}\text{C min}^{-1}$. All complexes display two obvious weight loss steps from 20 to 800 $^{\circ}\text{C}$ (figure S5). The TGA curve of **1** shows the first weight loss of 15.36% at 45–190 $^{\circ}\text{C}$, corresponding to elimination of lattice water and coordinated water (calcd: 15.55%). The second weight loss is observed from 375 to 450 $^{\circ}\text{C}$ demonstrating the loss of 4-dpyh and 1,2-BDC. The remaining weight, 16.85%, corresponds to the percentage (calcd: 17.28%) of Cu and O components. For **2**, the first weight loss of 3.26% at 106–168 $^{\circ}\text{C}$ indicates the exclusion of lattice water molecules (calcd:

3.15%). The coordination framework decomposes from 420 to 595 °C, corresponding to loss of 4-dpyh and 1,3-BDC with CuO of 14.14% (calcd: 13.98%) as residue. The TGA curve of **3** shows the first weight loss of 10.70% (34–254 °C), which indicates the exclusion of lattice and coordinated water (calcd: 10.94%). The second weight loss starting at 297 °C can be attributed to decomposition of organic ligands, and the residue is CdO (obs. 25.50%, calcd: 25.92%). For **4**, the first weight loss of 8.68% (calcd: 8.85%) at 52–131 °C reveals the release of lattice water. The second weight loss at 328 °C may be attributed to loss of organic ligands. The final solid product holds a weight of 12.84% of the total sample, which is in agreement with the ZnO (calcd: 13.28%).

3.7. Electrochemical behaviors of 1-CPE and 2-CPE

To study the electrochemical behaviors of Cu(II) complexes, carbon paste electrodes bulk modified with **1** and **2** (1-CPE and 2-CPE) are fabricated as the working electrodes due to their insolubility in water or common organic solvents. Compared with other film-modified electrodes, the bulk-modified CPEs show long term stability and especially good surface renewability by simple mechanical polishing in the event of surface fouling, which is important in practical application [16, 34]. The cyclic voltammograms of the 1-CPE and 2-CPE are obtained in 0.01 M H₂SO₄ + 0.5 M Na₂SO₄ aqueous solution (figure 5). From 450 to –300 mV or 320 to –220 mV, there is no redox peak at bare CPE. While for 1-CPE or 2-CPE, a reversible redox peak ascribed to Cu^{II}/Cu^I is observed [34, 35]. The mean peak potentials $E_{1/2} = (E_{pa} + E_{pc})/2$ are 75 mV for 1-CPE, and 60 mV for 2-CPE (scan rate: 50 mV s^{–1}).

The effects of scan rates on the electrochemical behavior of 1-CPE and 2-CPE are also studied in 0.01 M H₂SO₄ + 0.5 M Na₂SO₄ aqueous solution, as shown in figure 5. When the scan rates increase from 20 to 200 mV s^{–1}, the peak potentials of the 1-CPE (or 2-CPE) change gradually: the cathodic peak potentials shift to the negative direction and the corresponding anodic peak potentials shift to the positive direction. The plots of peak currents versus scan rates are shown in figure S6. The anodic and cathodic peak currents were proportional to the scan rates, indicating that the redox processes for 1-CPE and 2-CPE are surface-controlled. The electrochemical behaviors of 1-CPE and 2-CPE are similar to that of other reported copper(II) compounds [16, 36], the difference of peak potentials may be assigned to the influences of organic ligands and structures of these copper(II) compounds.

Reduction of NO₂[–] is totally irreversible at a glassy carbon electrode in acidic aqueous solution and does not take place prior to evolution of hydrogen [34, 37]. However, the reduction of NO₂[–] can readily be catalyzed by 1-CPE or 2-CPE in 0.01 M H₂SO₄ + 0.5 M Na₂SO₄ aqueous solution. As shown in figures S7 and S8, the comparative cyclic voltammograms for the electroreduction of KNO₂ at the surface of bare CPE and 1-CPE/or 2-CPE. Upon addition of KNO₂, there were dramatic enhancement of the cathodic peak currents and the anodic peak currents decreased, which indicate that 1-CPE and 2-CPE exhibit excellent electrocatalytic activities toward the reduction of KNO₂.

3.8. Fluorescent properties of 1–4

The fluorescent properties of **1–4**, together with the free bis-pyridyl-bis-amide ligands, were studied in the solid state at room temperature. The emission spectra of the compounds and free 4-dpyh and 3-dpyh are depicted in figure 6. The ligand 4-dpyh shows an intense

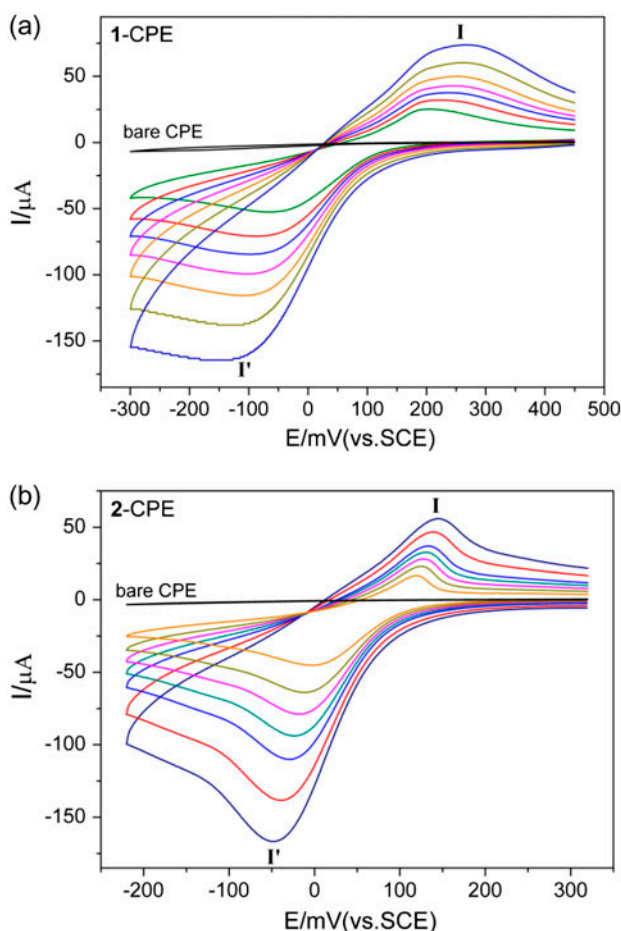


Figure 5. Cyclic voltammograms of bare CPE, (a) **1**-CPE (+450 to -300 mV) and (b) **2**-CPE (+320 to -220 mV) in 0.01 M H₂SO₄ + 0.5 M Na₂SO₄ aqueous solution at different scan rates (from inner to outer: 20, 50, 70, 90, 110, 150, and 200 mV s⁻¹).

emission at 379 nm ($\lambda_{\text{ex}} = 310$ nm). As for 3-dpyh, a strong fluorescent emission band at 400 nm ($\lambda_{\text{ex}} = 320$ nm) is observed. However, it was considered that the carboxylate ligands have no significant contribution to the fluorescent emission of the coordination polymers with the presence of the N-donor ligand. Thus, the emissions of the organic ligands may be ascribed to the $\pi^* \rightarrow \pi$ or $\pi^* \rightarrow n$ transitions [38, 39]. Compounds **1** and **2** both exhibit emission bands at 399 nm with excitation bands at 310 nm, comparing with the free 4-dpyh, which produce 20-nm red-shift in the fluorescent properties [figure 6(a)]. As for **3** and **4**, strong emission peaks at 375 and 414 nm are found ($\lambda_{\text{ex}} = 320$ nm) [figure 6(b)], blue-shifted 25 nm for **3** and red-shifted 14 nm for **4** compared with the peaks of 400 nm for free 3-dpyh. As to the d¹⁰ valence electron configuration of Cu(II)/Cd(II)/Zn(II) ion, the emission band of the Cu(II)/Cd(II)/Zn(II) compounds may be assigned to the LLCT, admixing with the LMCT as previously reported [40–42].

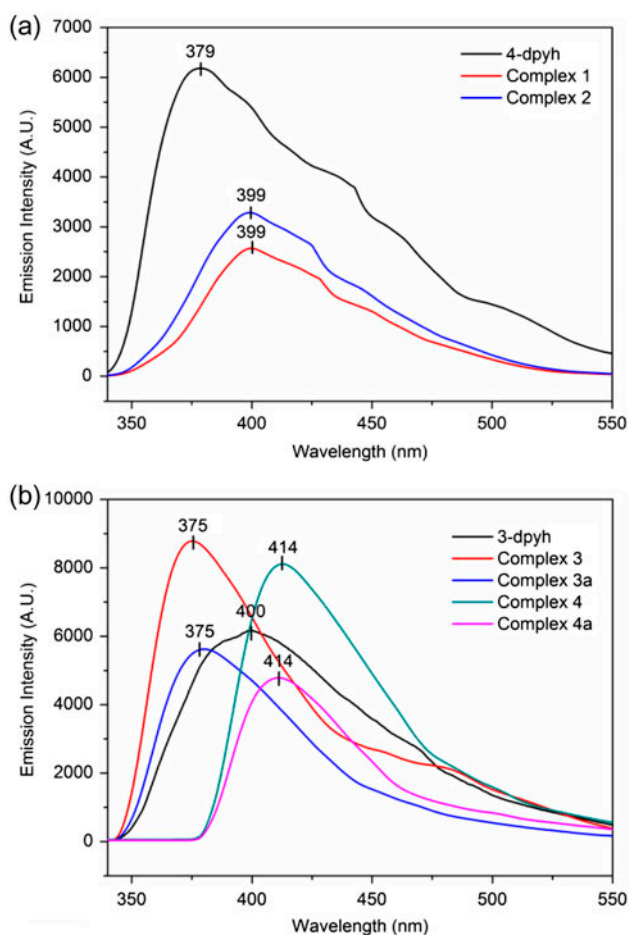


Figure 6. (a) The fluorescent emission spectra of **1**, **2** and free 4-dpyh; (b) the fluorescent emission spectra of **3** and **4**, powder samples of **3a** and **4a**, (the guest-free form of **3** and **4**) and free 3-dpyh.

3.9. Fluorescent selectivity of **3** and **4**

Fluorescence spectra recorded on powder samples of **3a** and **4a** (the guest-free form of **3** and **4**) revealed fluorescent quenching behavior [figure 6(b)], which may be attributed to the disappearance of the interactions between their frameworks and lattice water molecules. Desolvated **3a** and **4a** were prepared as follows: after immersing in CH₃OH for three days, the sample was evacuated at 60 °C for 1 h and then 120 °C for over 3 h. The fluorescent properties of **3a** and **4a** in various solvent emulsions (designated as **3a**-solvent and **4a**-solvent, respectively) were studied at room temperature. The **3a**-solvent and **4a**-solvent emulsions were prepared by introducing 5.0 mg of **3a** and **4a** powders into 5.0 mL of CH₃OH, CH₃CH₂OH, CH₃CN, CH₂Cl₂, DMF, DMSO, THF, distilled water, diethyl ether, or cyclohexane, respectively. After sonication, aging for over 24 h and shaking, filtering, and drying in air, the fluorescent spectra were measured. As shown in figure 7, when desolvated **3a** was prepared by **3a**-CH₃OH or **3a**-CH₃CN, the fluorescent intensity was increased.

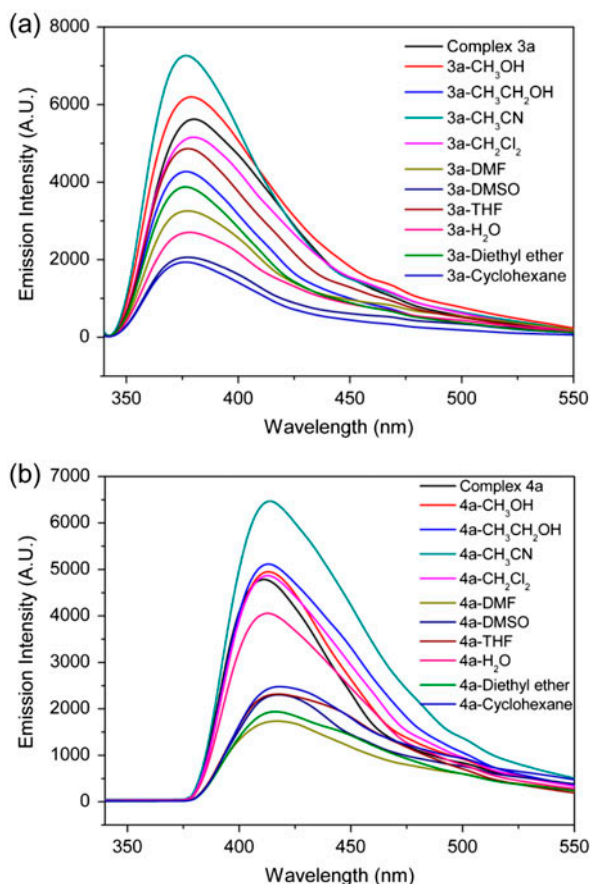


Figure 7. The fluorescent spectra of (a) **3a**-solvent and (b) **4a**-solvent in various pure solvents.

In contrast, the addition of other organics, such as $\text{CH}_3\text{CH}_2\text{OH}$, CH_2Cl_2 , DMF, DMSO, THF, distilled water, diethyl ether, or cyclohexane, the different degrees of fluorescent quenching can be observed. While the desolvated **4a** was obtained by **4a-CH₃OH/CH₃CH₂OH/CH₃CN/CH₂Cl₂**, the fluorescent intensities increased, but the additions of other organic solvents lead to the fluorescent quenching. In all of these organic solvents, the fluorescent enhancements of **3** and **4** in CH_3CN were significant. For **3**, the fluorescent intensity was the lowest in cyclohexane, while the lowest fluorescent emission was in DMF for **4**. The fluorescence spectra of **3a** and **4a** displayed unique fluorescent quenching and enhancement behaviors upon immersing in various solvent emulsions, revealing that different solvents as guest molecules in the voids of network **3a** or **4a** display an effect on their fluorescence intensity, which is similar to previous reports [43, 44]. The results indicate that **3** and **4** may be applied as fluorescent probes for some small solvent molecules with excellent fluorescent sensing activities.

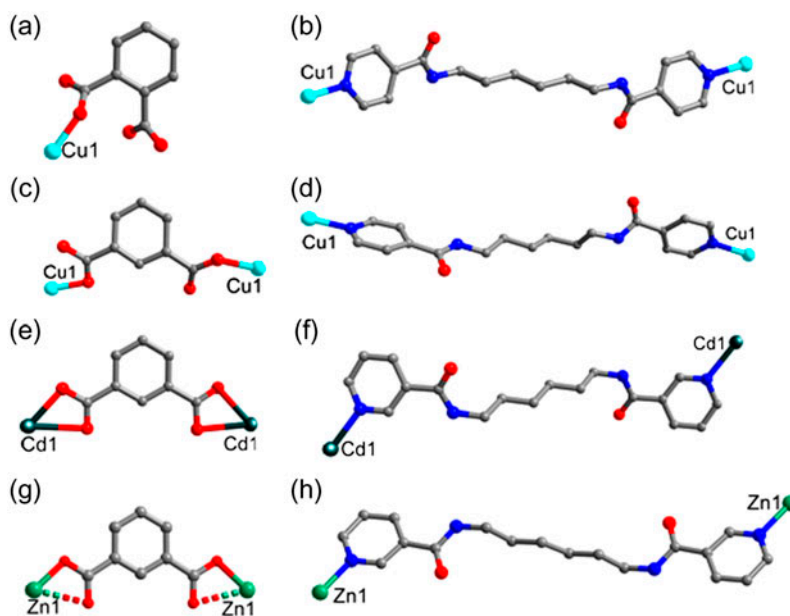


Chart 1. Coordination modes of 1,2-BDC (a), 1,3-BDC (c, e, g), 4-dpyh (b, d) and 3-dpyh (f, h) in 1–4.

4. Conclusion

We have synthesized four new metal–organic compounds in the mixed ligands system of aromatic dicarboxylates (1,2-BDC or 1,3-BDC) and the flexible bis-pyridyl-bis-amide ligands (4-dpyh or 3-dpyh), formulated as $[\text{Cu}(4\text{-dpyh})_{0.5}(\text{1,2-BDC})(\text{H}_2\text{O})_3] \cdot \text{H}_2\text{O}$ (**1**), $[\text{Cu}(4\text{-dpyh})(\text{1,3-BDC})(\text{H}_2\text{O})]$ (**2**), $[\text{Cd}(3\text{-dpyh})_{0.5}(\text{1,3-BDC})(\text{H}_2\text{O})_2] \cdot \text{H}_2\text{O}$ (**3**), and $[\text{Zn}(3\text{-dpyh})(\text{1,3-BDC})] \cdot 3\text{H}_2\text{O}$ (**4**). Compound **1** is a discrete dinuclear structure, **2** and **4** exhibit two different 2-D polymeric layers, and **3** possesses a 1-D ribbon chain structure. The structures illustrate the influences of central metal ions and dicarboxylates with different positions of carboxyl groups. Moreover, the electrochemical behaviors of **1** and **2** modified carbon paste electrodes indicate that **1** and **2** may be potential candidates for electrochemical materials. Our fluorescent studies on the guest-free forms of **3** and **4** (**3a** and **4a**) demonstrated that they could be potential fluorescent probes for detecting solvent molecules. Further work for preparing new coordination compounds with novel structures and special applications based on other flexible bis-pyridyl-bis-amide ligands is in progress.

Supplementary material

Crystallographic data for the structures reported in this paper have been deposited in the Cambridge Crystallographic Data Center with CCDC Numbers 905475 for **1**, 970646 for **2**, 20055 for **3** and 920056 for **4**. These data can be obtained free of charge from the Cambridge Crystallographic Data Center via www.ccdc.cam.ac.uk/data_request/cif.

Funding

This work was supported by the National Natural Science Foundation of China [grant number 20871022], [grant number 21171025]; New Century Excellent Talents in University [grant number NCET-09-0853]; the Natural Science Foundation of Liaoning Province [grant number 201102003]; Program of Innovative Research Team in University of Liaoning Province [grant number LT2012020].

References

- [1] Y.H. Fu, D.R. Sun, Y.J. Chen, R.K. Huang, Z.X. Ding, X.Z. Fu, Z.H. Li. *Angew. Chem. Int. Ed.*, **51**, 3364 (2012).
- [2] S. Wang, J.F. Bai, H. Xing, Y.Z. Li, Y. Song, Y. Pan, M.F. Scheer, X.Z. You. *Cryst. Growth Des.*, **7**, 747 (2007).
- [3] J. Yang, J.F. Ma, Y.Y. Liu, J.C. Ma, H.Q. Jia, N.H. Hu. *Eur. J. Inorg. Chem.*, **2006**, 1208 (2006).
- [4] L.Q. Mo, J.H. Jia, L.J. Sun, Q.M. Wang. *Chem. Commun.*, **48**, 8691 (2012).
- [5] C.P. Li, J. Chen, Q. Yu, M. Du. *Cryst. Growth Des.*, **10**, 1623 (2010).
- [6] Y.Q. Chen, G.R. Li, Z. Chang, Y.K. Qu, Y.H. Zhang, X.H. Bu. *Chem. Sci.*, **4**, 3678 (2013).
- [7] A.Y. Robin, K.M. Fromm. *Coord. Chem. Rev.*, **250**, 2127 (2006).
- [8] L.N. Li, J.H. Luo, S.Y. Wang, Z.H. Sun, T.L. Chen, M.C. Hong. *Cryst. Growth Des.*, **11**, 3744 (2011).
- [9] Z. Zhang, D.F. Wu, K. Hu, Y.J. Shi, Z.L. Chen, F.P. Liang. *J. Coord. Chem.*, **66**, 2499 (2013).
- [10] L.F. Ma, Q.L. Meng, L.Y. Wang, B. Liu, F.P. Liang. *Dalton Trans.*, **39**, 8210 (2010).
- [11] C.Y. Wang, Z.M. Wilseck, R.M. Supkowski, R.L. LaDuca. *CrystEngComm*, **13**, 1391 (2011).
- [12] L.F. Ma, J.W. Zhao, M.L. Han, L.Y. Wang, M. Du. *Dalton Trans.*, **41**, 2078 (2012).
- [13] X.X. Xu, Z.P. Cui, J. Qi, X.X. Liu. *Dalton Trans.*, **42**, 13546 (2013).
- [14] G.B. Li, L. Li, J.M. Liu, T. Yang, C.Y. Su. *Cryst. Growth Des.*, **13**, 1518 (2013).
- [15] F.X. Yue, X.Y. Yu, Y.H. Luo, J.J. Yang, X. Chen, H. Zhang. *J. Coord. Chem.*, **66**, 2843 (2013).
- [16] X.L. Wang, H.Y. Lin, B. Mu, A.X. Tian, G.C. Liu, N.H. Hu. *CrystEngComm*, **13**, 1990 (2011).
- [17] Z.M. Wilseck, C.M. Gandolfo, R.L. LaDuca. *Inorg. Chim. Acta*, **363**, 3865 (2010).
- [18] L.F. Ma, B. Liu, L.Y. Wang, C.P. Li, M. Du. *Dalton Trans.*, **39**, 2301 (2010).
- [19] X. Zhang, L. Hou, B. Liu, L. Cui, Y.Y. Wang, B. Wu. *Cryst. Growth Des.*, **13**, 3177 (2013).
- [20] Y.H. Yu, B. Wen, H.Z. Zhang, G.F. Hou, J.S. Gao, P.F. Yan. *J. Coord. Chem.*, **67**, 588 (2014).
- [21] H.L. Hu, Y.F. Hsu, C.J. Wu, C.W. Yeh, J.D. Chen, J.C. Wang. *Polyhedron*, **33**, 280 (2012).
- [22] J.J. Cheng, Y.T. Chang, C.J. Wu, Y.F. Hsu, C. Lin, D. Proserpio, J.D. Chen. *CrystEngComm*, **14**, 537 (2011).
- [23] Y. Gong, J. Li, J.B. Qin, T. Wu, R. Cao, J.H. Li. *Cryst. Growth Des.*, **11**, 1662 (2011).
- [24] S.Y. Huang, J.Q. Li, S.J. Liu, Y. Ning, L.N. Meng, J.Y. Li, M.B. Luo, F. Luo. *CrystEngComm*, **16**, 5608 (2014).
- [25] X.L. Wang, B. Mu, H.Y. Lin, G.C. Liu. *J. Organomet. Chem.*, **696**, 2313 (2011).
- [26] X.L. Wang, B. Mu, H.Y. Lin, S. Yang, G.C. Liu, A.X. Tian, J.W. Zhang. *Dalton Trans.*, **41**, 11074 (2012).
- [27] H.Y. Lin, P. Liu, J.W. Zhang, X.L. Wang, G.C. Liu. *J. Coord. Chem.*, **66**, 612 (2013).
- [28] X.L. Wang, P. Liu, H.Y. Lin, C. Xu, J.W. Zhang, G.C. Liu, A.X. Tian. *Inorg. Chem. Commun.*, **30**, 79 (2013).
- [29] S. Muthu, J.H.K. Yip, J.J. Vittal. *J. Chem. Soc., Dalton Trans.*, 4561 (2002).
- [30] G.M. Sheldrick. *Acta Crystallogr. Sect. A*, **64**, 112 (2008).
- [31] X.L. Wang, J. Luan, H.Y. Lin, Q.L. Lu, C. Xu, G.C. Liu. *Dalton Trans.*, **42**, 8375 (2013).
- [32] T.V. Mitkina, N.F. Zakharchuk, D.Y. Naumov, O.A. Gerasko, D. Fenske, V.P. Fedin. *Inorg. Chem.*, **47**, 6748 (2008).
- [33] D. Zhao, Y. Xiu, X.L. Zhou, X.R. Meng. *J. Coord. Chem.*, **65**, 112 (2012).
- [34] X.L. Wang, H.Y. Zhao, H.Y. Lin, G.C. Liu, J.N. Fang, B.K. Chen. *Electroanalysis*, **20**, 1055 (2008).
- [35] G.G. Gao, L. Xu, W.J. Wang, W.J. An, Y.F. Qiu, Z.Q. Wang, E.B. Wang. *J. Phys. Chem. B*, **109**, 8948 (2005).
- [36] V.T. Kasumov, A. Bulut, F. Köksal, M. Aslanog˘lu, İ. Uçar, C. Kazak. *Polyhedron*, **25**, 1133 (2006).
- [37] Y. Gong, T. Wu, J.H. Lin. *CrystEngComm*, **14**, 3727 (2012).
- [38] C.Y. Xu, L.K. Li, Y.P. Wang, Q.Q. Guo, X.J. Wang, H.W. Hou, Y.T. Fan. *Cryst. Growth Des.*, **11**, 4667 (2011).
- [39] L.J. Zhang, D.H. Xu, Y.S. Zhou, Y. Guo, W. Ahmad. *J. Coord. Chem.*, **65**, 3028 (2012).
- [40] S.S. Chen, Y. Zhao, J. Fan, T.A. Okamura, Z.S. Bai, Z.H. Chen, W.Y. Sun. *CrystEngComm*, **14**, 3564 (2012).
- [41] P.-F. Yao, C.-J. Ye, F.-P. Huang, H.-D. Bian, Q. Yu, K. Hu. *J. Coord. Chem.*, **66**, 1591 (2013).
- [42] H.W. Kuai, T.A. Okamura, W.Y. Sun. *J. Coord. Chem.*, **65**, 3147 (2012).
- [43] G.L. Liu, Y.J. Qin, L. Jing, G.Y. Wei, H. Li. *Chem. Commun.*, **49**, 1699 (2013).
- [44] G.Y. Wang, L.L. Yang, Y. Li, H. Song, W.J. Ruan, Z. Chang, X.H. Bu. *Dalton Trans.*, **42**, 12865 (2013).